IJE TRANSACTIONS A: Basics Vol. 37 No. 07, (July 2024) 1306-1316

International Journal of Engineering

Journal Homepage: www.ije.ir

Enhancing Wind Power Conversion System Control Under Wind Constraints Using Single Hidden Layer Neural Network

A. Mazari*[a], H. Ait Abbas[b], K. Laroussi[a], B. Naceri[c]

[a] *Laboratory of Applied and Automation and Industrial Diagnostic (LAADI), University of Djelfa, Djelfa, Algeria*
[b] *Laboratory of Electrical and Automatic Systems Engineering (LGSEA), University of Bouira, Bouira, Algeria*
[c] *Laboratory of Identification, Commande, Control and Communication (LI3CUB), University of Biskra, Algeria*

P A P E R I N F O

Paper history:
Received 27 November 2023
Received in revised form 25 December 2023
Accepted 10 January 2024

Keywords:
Wind Power Generation System
Cascaded Doubly Fed Induction Generator
Proportional Integral Derivative
Single Hidden Layer Neural Network

A B S T R A C T

In the realm of wind power generation, cascaded doubly fed induction generators (CDFIG) play a pivotal role. However, the classical proportional integral derivative (PID) controllers used within such systems often struggle with instability and inaccuracies arising from wind variability. This study proposes an enhancement to overcome these limitations by incorporating a single hidden layer neural network (SHLNN) into the wind power conversion systems (WPCS). The SHLNN aims to complement the PID controller by addressing its shortcomings in handling nonlinearities and uncertainties. This integration exploits the adaptive nature and low computational demand of SHLNNs, utilizing historical wind speed and power data to form a more resilient control strategy. Through Matlab/Simulink simulations, this approach is rigorously compared against traditional PID control methods. The results demonstrate a marked improvement in performance, highlighting the SHLNN's capacity to contend with the intrinsic variabilities of wind patterns. This contribution is significant as it offers a sophisticated yet computationally efficient solution to enhance CDFIG-based WPCS, ensuring more stable and accurate energy production.

***doi**: 10.5829/ije.2024.37.07a.10*

Graphical Abstract

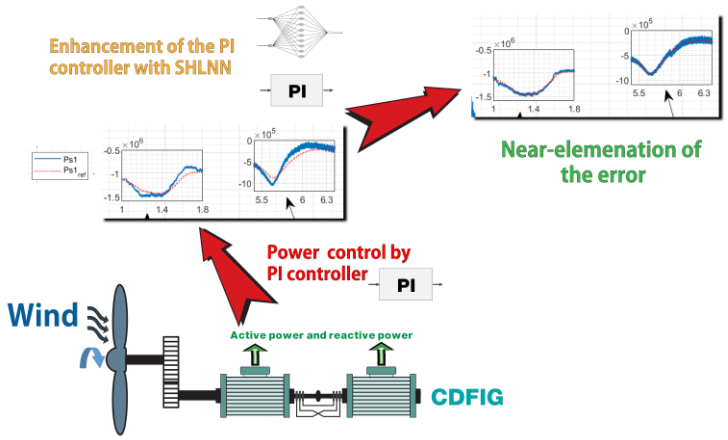

NOMENCLATURE

C_p	Power coefficient	w_{ij}	Weights between the second and the third layer
F_{dq}, k_{dq}	Adaptation gains	x_k	Input of neural network

* Corresponding Author Email: ali.mazari@univ-djelfa.dz (A. Mazari)

Please cite this article as: Mazari A, Ait Abbas H, Laroussi K, Naceri B. Enhancing Wind Power Conversion System Control Under Wind Constraints Using Single Hidden Layer Neural Network. International Journal of Engineering, Transactions A: Basics. 2024;37(07):1306-16.

L_{m1}, L_{m2}	Mutual inductanses [H]	y_{nn}	Output of neural network
L_{r1}, L_{r2}	Inductances of the first and the second rotor [H]	μ_d, μ_q	Neural network inputs in d-q axis
L_{s1}, L_{s2}	Inductances of the first and the second stator [H]	G	Gearbox's gain
P_{s1}	Active power of the first generator [W]	C	Constante
P_t	Aerodynamic power [W]	I	Unit matrix
Q_{s1}	Reactive power of the first generator [W]	J	Equation of jacoby
R_{s1}	First stator resistance [ohm]	V	Weights matrix for the hidden layer
R_{s2}	Second stator resistance [ohm]	W	Weights matrix
R_t	The blade length [m]	e	Error
T_{em}	Electromagnetic torque [N.m]	f	Friction of the wind turbine [N.m/(rad/s)]
T_g	Generator side torque [N.m]	j	Inertia of the wind turbine [kg.m^2]
T_t	Aerodynamic torque [N.m]	**Greek Symbols**	
$\hat{V}$	Estimate matrix for V	$\tilde{\imath}_{dq}$	Dynamic error
V_0	Primary value of V	Δ_d, Δ_q	Target terms in d-q axis
V_s	Grid voltage	Ω_{mec}	Mechanical speed of the generator [rad/s]
$\widehat{W}$	Estimate matrix for the W	Ω_t	Rotational speed of the wind turbine [rad/s]
W_0	Primary value of W	τ_r	Response time [s]
W_{k+1}, W_k	Results of calculated weights by Gauss-Newton	$\varphi_{dr1}, \varphi_{qr1}$	First rotor fluxes in d-q axis [WB]
i_{dr}, i_{qr}	Rotor currents in d-q axis [A]	$\varphi_{dr2}, \varphi_{qr2}$	second rotor fluxes in d-q axis [WB]
i_{ds1}, i_{qs1}	First stator currents in d-q axis [A]	$\varphi_{ds1}, \varphi_{qs1}$	First stator fluxes in d-q axis [WB]
i_{ds2}, i_{qs2}	Second stator currents in d-q axis [A]	$\varphi_{ds2}, \varphi_{qs2}$	Second stator fluxes in d-q axis [WB]
k_i, k_p	PI regulator's gains	$\varphi_j(.)$	Activation function
p_1, p_2	Number of poles of the first and the second generator	ω_{r1}, ω_{r2}	Angular frequency of the first and the second rotor
s_1, s_2	Slips of the first and the second generator	ω_{s1}, ω_{s2}	Angular frequency of the first and the second stator
u_Δ	Adaptive term	ϑ_{vj}	Biases between the first and the second layer
u_{ad}, u_{aq}	Adaptive terms in d-q axis	ϑ_{wi}	Biases between the second and the third layer
v_{ds1}, v_{qs1}	First stator voltages in d-q axis [V]	β	Pitch angle [°]
v_{ds2}, v_{qs2}	Second stator voltages in d-q axis [V]	λ	Velocity ratio
v_{jk}	Weights between the first and the second layer	μ	Positive coefficient
v_w	Wind velocity [m/s]	ρ	Air density [kg/m^3]

1. INTRODUCTION

As societies increasingly depend on electrical energy, there has been a notable rise in the utilization of renewable energy sources like wind power (1). This trend is primarily driven by the urgent need to lessen reliance on fossil fuels and mitigate the environmental impact caused by traditional energy sources (2).

Within the realm of wind power, one promising technology is the cascaded doubly fed induction generator (CDFIG) system (3). This innovative system combines two doubly fed induction generators (DFIGs) while preserving their original design (3, 4). It involves coupling two wound rotor induction generators at their rotor windings, both mounted on a shared shaft (3, 5, 6). Compared to traditional wind power systems, the CDFIG system offers several advantages, including enhanced reliability and reduced maintenance costs (7). One key benefit of employing CDFIG system is its ability to operate at variable speeds (4, 6). This is particularly valuable as it effectively stabilizes the generator voltage frequency when fluctuations occur in the rotor speed (6).

There has been a growing trend in recent years to integrate intelligent techniques in WPCS (8). Artificial neural networks (ANNs) are widely recognized as a fundamental, powerful, and efficient approach for creating control strategies in situations where systems are only partially understood and have complex mathematical models (9). ANNs possess the capability to learn and approximate the dynamics of nonlinear systems by utilizing available input and output information (10). They are commonly applied in the fields of identification, adaptive control, and observation (11).

The literature encompasses various control techniques employed in wind power conversion systems (WPCS) utilizing the cascaded doubly fed induction generator (CDFIG). Notable examples include direct torque and flux control (12), sliding mode control (SMC) as described by Maafa et al. (7) and Zahedi et al. (13), This control technique frequently encounters undesired chattering phenomena (14). However, this phenomena can be decreased by updating the traditional SMC into the terminal SMC by Abdolhadi et al. (15) and the super-twisting SMC by Yan and Cheng (16) but it leads to more complexity of the controller (17). The predictive torque control of CDFIG highlighted by Bayhan et al. (18) which focuses on directly controlling the torque or flux, and the predictive voltage control also by Abdolrahimi

and Arab Khaburi (19). Dauksha and Iwanski (20) an indirect torque control algorithm for a CDFIG that allows it to work with an unbalanced power grid using different strategies. The development of an intelligent LAMDA-based controller for three-phase induction motors has shown improved precision and disturbance response by Morales et al. (21). Additionally, studies on the behavior of wind turbine blades in different turbulence levels have underscored the necessity for durable designs in renewable energy technologies (22). In finance, the integration of time-series analysis into neural network models has significantly enhanced stock price prediction accuracy (23). Our contribution aims to combine the strengths of the CDFIG with intelligent technique in the WPCS by integrating SHLNN which provides low computing complexity and good adaptation abilities to the control system.

This research identifies a gap in the existing literature regarding a control system that effectively manages these nonlinearities and uncertainties without introducing additional complexity. To address this gap, the article proposes a control strategy that integrates a single hidden layer neural network (SHLNN) with a PI controller. The SHLNN is designed to complement the PI controller by enhancing its adaptive capabilities while maintaining a low computational footprint.

The paper presents a detailed exposition of the mathematical model of the WPGS encompassing the CDFIG and the wind turbine models, the controller of the active power and reactive power of CDFIG designed including field-oriented control with PI controller in the first case then the implementation of the SHLNN alongside with a PI controller in the second case. Subsequently, applying the control methods in the WPGS and discussing the simulation results by comparing both cases. The paper concludes with a summary of the findings and their implications for future research in the wind power generation systems.

2. MATHEMATICAL MODEL OF THE WPCS

2. 1. Model of The CDFIG The two doubly fed induction generators are connected mechanically and electrically, their stator windings are electrically isolated from each other, their rotors are connected to the same shaft, and the rotor circuits are linked with a reverse phase sequence (24). These generators are referred to the first generator as the control generator (CG) and the second as the power generator (PG) (24), as shown in Figure 1:

By employing a commonly used DFIG model and assuming symmetrical electrical circuits for both the first generator and the second generator across all phases (20), the rotor windings of the two generators are interconnected in opposite connection, this linkage gives

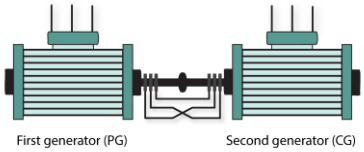

Figure 1. The cascaded doubly fed induction generator

the following model in d-q axis (13, 25):

$$v_{ds1} = R_{s1}i_{ds1} + L_{s1}\frac{di_{ds1}}{dt} + L_{m1}\frac{di_{dr}}{dt} - \omega_{s1}L_{s1}i_{qs1} - \omega_{s1}L_{m1}i_{qr} \quad (1)$$

$$v_{qs1} = R_{s1}i_{qs1} + L_{s1}\frac{di_{qs1}}{dt} + L_{m1}\frac{di_{qr}}{dt} + \omega_{s1}L_{s1}i_{ds1} + \omega_{s1}L_{m1}i_{dr} \quad (2)$$

$$0 = R_r i_{dr} + L_r\frac{di_{dr}}{dt} + L_{m1}\frac{di_{ds1}}{dt} - \omega_{g1}L_r i_{qr} - \omega_{g1}L_{m1}i_{qs1} - L_{m2}\frac{di_{ds2}}{dt} + \omega_{g1}L_{m2}i_{qs2} \quad (3)$$

$$0 = R_r i_{qr} + L_r\frac{di_{qr}}{dt} + L_{m1}\frac{di_{qs1}}{dt} + \omega_{g1}L_r i_{dr} + \omega_{g1}L_{m1}i_{ds1} - L_{m2}\frac{di_{qs2}}{dt} - \omega_{g1}L_{m2}i_{ds2} \quad (4)$$

$$v_{ds2} = R_{s2}i_{ds2} + L_{s2}\frac{di_{ds2}}{dt} - L_{m2}\frac{di_{dr}}{dt} - \omega_{s2}L_{s2}i_{qs2} + \omega_{s2}L_{m2}i_{qr} \quad (5)$$

$$v_{qs2} = R_{s2}i_{qs2} + L_{s2}\frac{di_{qs2}}{dt} - L_{m2}\frac{di_{qr}}{dt} + \omega_{s2}L_{s2}i_{ds2} - \omega_{s2}L_{m2}i_{dr} \quad (6)$$

The fluxes (25):

$$\varphi_{ds1} = L_{s1}i_{ds1} + L_{m1}i_{dr1} \quad (7)$$

$$\varphi_{qs1} = L_{s1}i_{qs1} + L_{m1}i_{qr1} \quad (8)$$

$$\varphi_{dr1} = L_{r1}i_{dr1} + L_{m1}i_{ds1} \quad (9)$$

$$\varphi_{qr1} = L_{r1}i_{qr1} + L_{m1}i_{qs1} \quad (10)$$

$$\varphi_{ds2} = L_{s2}i_{ds2} + L_{m2}i_{dr2} \quad (11)$$

$$\varphi_{qs2} = L_{s2}i_{qs2} + L_{m2}i_{qr2} \quad (12)$$

$$\varphi_{dr2} = L_{r2}i_{dr2} + L_{m2}i_{ds2} \quad (13)$$

$$\varphi_{qr2} = L_{r2}i_{qr2} + L_{m2}i_{qs2} \quad (14)$$

The frequency response of both stators and rotors is provided as follows (26):

$$\omega_{g1} = \omega_{g2} = \omega_{s1} - \omega_{r1} \quad (15)$$

$$\omega_{s2} = \omega_{s1} - \omega_{r1} - \omega_{r2} \quad (16)$$

$$\omega_{r1} = p_1\Omega \quad (17)$$

The total electromagnetic torque (T_{em}) of the cascade is determined by the addition of the torques generated by the two individual generators (25):

$$T_{em} = p_1 L_{m1}(i_{dr} i_{qs1} - i_{ds1} i_{qr}) + p_2 L_{m2}(i_{dr} i_{qs2} - i_{ds2} i_{qr}) \quad (18)$$

2. 2. Modeling of The Wind Turbine The wind turbine harnesses the kinetic energy of the wind, resulting in the rotation of its blades and the conversion of this energy into mechanical energy, which drives the rotor of the generator. The aerodynamic power (P_t) and torque (T_t) associated with this process are represented by the following expression (27):

$$P_t = \frac{1}{2} C_p(\lambda, \beta) \rho R_t \pi v_w^3 \quad (19)$$

$$T_t = \frac{P_t}{\Omega_t} \quad (20)$$

The power coefficient is given by Kelkoul and Boumediene (28):

$$C_p = (0.3 - 0.0167\beta)\, sin\left(\frac{\pi(\lambda+0.1)}{10-0.3\beta}\right) - 0.00184(\lambda - 3)\beta \quad (21)$$

The gearbox serves to connect the generator and the wind turbine, amplifying the rotational speed transmitted from the wind turbine. The relationship between the rotational speed of the generator and that of the wind turbine is defined as follows (27, 28):

$$\Omega_t = \frac{\Omega_{mec}}{G} \quad (22)$$

The fundamental equation that governs the dynamics of speed and torques can be expressed as follows (27, 28):

$$j \frac{d\Omega_{mec}}{dt} + f\Omega_{mec} = T_g - T_{em} \quad (23)$$

3. CONTROL OF THE CDFIG

3. 1. Field Oriented Control It is a naturalistic separation between the magnitude associated with the flux (the excitation current) and that related to the torque (the armature current), which makes the delay of torque response decrease and increase the speed control rang. Hence, a higher efficiency over a long-term steady state load (9).

The initial stator flux φ_{s1} is aligned with the d-axis. When traversing along the q-axis, the flux of the first stator remains consistently at zero (5).

$$\varphi_{ds1} = \varphi_{s1} \quad (24)$$

$$\varphi_{qs1} = 0 \quad (25)$$

By considering the resistance of the first stator neglected, the voltages can be simplified as follows:

$$v_{ds1} = 0 \quad (26)$$

$$v_{qs1} = V_s = \omega_{s1} \varphi_{s1} \quad (27)$$

The voltages of the second stator in relation with the currents, the first stator currents in relation with those of the second stator. Hence, the active and reactive powers are described by Maafa et al. (25):

$$v_{ds2} = R_{s2} i_{ds2} + (L_{s2} - C.L_{m2}) \frac{di_{ds2}}{dt} - s.\omega_{s1}(L_{s2} - C.L_{m2}) i_{qs2} \quad (28)$$

$$v_{qs2} = R_{s2} i_{qs2} + (L_{s2} - C.L_{m2}) \frac{di_{qs2}}{dt} + s.\omega_{s1}(L_{s2} - C.L_{m2}) i_{ds2} + C.s \frac{L_{m1}.V_s}{L_{s1}} \quad (29)$$

$$i_{ds1} = \frac{V_s}{\omega_{s1}.L_{s1}} \left(1 + \frac{C.{L_{m1}}^2}{L_{s1}.L_{m2}}\right) - C.\frac{L_{m1}}{L_{s1}} i_{ds2} \quad (30)$$

$$i_{qs1} = -C.\frac{L_{m1}}{L_{s1}} i_{qs2} \quad (31)$$

$$P_{s1} = -C.V_s \frac{L_{m1}}{L_{s1}} i_{qs2} \quad (32)$$

$$Q_{s1} = \frac{{V_s}^2}{\omega_{s1}.L_{s1}} \left(1 + \frac{C.{L_{m1}}^2}{L_{s1}.L_{m2}}\right) - C.V_s \frac{L_{m1}}{L_{s1}} i_{ds2} \quad (33)$$

$$C = \frac{L_{m2}}{L_{r1} + L_{r2} - \frac{{L_{m1}}^2}{L_{s1}}} \quad (34)$$

$$s = s_1.s_2 = \frac{\omega_{s1} - \Omega(p_1 + p_2)}{\omega_{s1}} \quad (35)$$

The first stator's active and reactive powers (P_{s1}, Q_{s1}) will be the output signals from the CDFIG that will be controlled to achieve the tracking reliability of energy in the WPCS.

3. 2. PI Controller The speed control loop, PI regulator structure is illustrated in Figure 2. The design is based on the dynamic equation governing the behavior of the rotating components:

The open-loop transfer function is expressed as follows:

$$\frac{Y}{Y_{ref}} = \frac{P + \frac{k_i}{P}}{\frac{P}{k_p}} \frac{\frac{C.L_{m1}.V_S}{L_{s1}(L_{s2} - C.L_{m2})}}{P + \frac{R_{S2}}{(L_{s2} - C.L_{m2})}} \quad (36)$$

Several approaches are used to calculate the parameters k_i and k_p (29), by using the poles compensation approach, the closed-loop transfer function is obtained

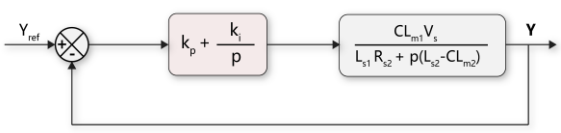

Figure 2. PI regulator structure

as follows:

$$\frac{Y}{Y_{ref}} = \frac{1}{1+P\frac{L_{s1}(L_{s2}-C.L_{m2})}{k_p.C.L_{m1}.V_s}} \quad (37)$$

$$\frac{k_i}{k_p} = \frac{R_{s2}}{(L_{s2}-C.L_{m2})} \quad (38)$$

The gains of PI regulator are distinguished by:

$$k_p = \frac{L_{s1}(L_{s2}-C.L_{m2})}{\tau_r.C.L_{m1}.V_s} \quad (39)$$

$$k_i = k_p \frac{R_{s2}}{(L_{s2}-C.L_{m2})} = \frac{L_{s1}.R_{s2}}{\tau_r.C.L_{m1}.V_s} \quad (40)$$

$$\tau_r = \frac{1}{1+P\frac{L_{s1}(L_{s2}-C.L_{m2})}{k_p.C.L_{m1}.V_s}} \quad (41)$$

3. 3. Adaptive Control Architecture In order to benefit the advantages of neural networks (NN) in power control of the CDFIG, we will incorporate two blocks of SHLNN alongside PI controllers. The first block will be utilized in the d-axis, associated with reactive power Q, and the second block in the q-axis, associated with active power P. The purpose of integrating these components is to enable the calculation of adaptive terms that actively influence our system, with the goal of minimizing tracking errors.

By implementing the SHLNN blocks on the d-axis and q-axis, we enhance the capability of our power control system. The SHLNN utilizes its neural network architecture to learn and adapt to varying operating conditions. It analyzes input data, such as voltage and current measurements, and produces adaptive terms u_{ad} and u_{aq}, that can be used to adjust the control signals for the CDFIG.

Inputs of NN blocks are:

- For the d-axis: $[V_{ds2};\ Q_{s1}]$
- For the q-axis: $[V_{qs2};\ P_{s1}]$

The outputs are Δ_d for d-axis and Δ_q for q-axis, which are considered as targets.

$$\frac{di_{ds2}}{dt} = v_{ds2} + \Delta_d \quad (42)$$

$$\frac{di_{qs2}}{dt} = v_{qs2} + \Delta_q \quad (43)$$

From Equations 5 and 6 we have:

$$\frac{di_{ds2}}{dt} = \frac{v_{ds2}}{L_{s2}} + \frac{1}{L_{s2}}\left(-R_{s2}i_{ds2} + L_{m2}\frac{di_{dr}}{dt} + \omega_{s2}L_{s2}i_{qs2} - \omega_{s2}L_{m2}i_{qr}\right) \quad (44)$$

$$\frac{di_{qs2}}{dt} = \frac{v_{qs2}}{L_{s2}} + \frac{1}{L_{s2}}\left(-R_{s2}i_{qs2} + L_{m2}\frac{di_{qr}}{dt} - \omega_{s2}L_{s2}i_{ds2} + \omega_{s2}L_{m2}i_{dr}\right) \quad (45)$$

From Equation 37 The outputs can be distinguished as follows:

$$\Delta_d = \frac{1}{L_{s2}}\left(-R_{s2}i_{ds2} + L_{m2}\frac{di_{dr}}{dt} + \omega_{s2}L_{s2}i_{qs2} - \omega_{s2}L_{m2}i_{qr}\right) \quad (46)$$

$$\Delta_q = \frac{1}{L_{s2}}\left(-R_{s2}i_{qs2} + L_{m2}\frac{di_{qr}}{dt} - \omega_{s2}L_{s2}i_{ds2} + \omega_{s2}L_{m2}i_{dr}\right) \quad (47)$$

Figure 3 shows the adaptive controller architecture of the CDFIG:

3. 4. Neural network Approximation Within a feedforward neural network, information exclusively goes in a singular direction, progressing from the input layer to the output layer, without any reverse propagation (30). In the context of controlling nonlinear systems, neural networks (NNs) are commonly utilized as adaptive components to offset the impact of uncertainties present within the system. These uncertainties can include unaccounted dynamics, parameters that vary with time, and errors in modeling. NNs are favored for this purpose due to their remarkable capability to approximate continuous mappings of real values, provided that an appropriate NN architecture is employed (11), the general structure of NN is shown in Figure 4.

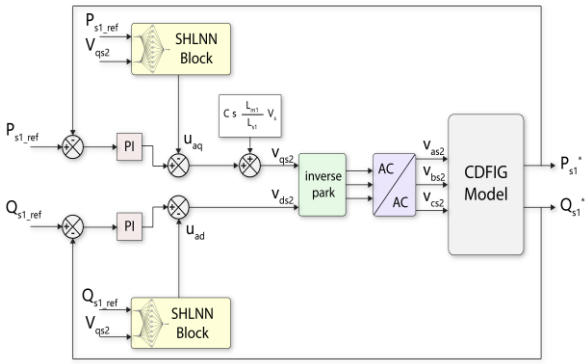

Figure 3. The adaptive control architecture of the CDFIG

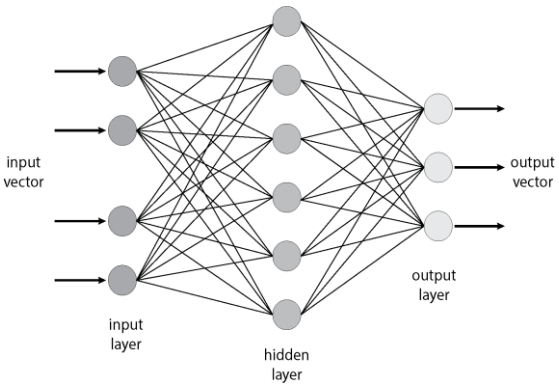

Figure 4. The structure of a single hidden layer neural network

The relation between the input and the output of a SHLNN is given by Rahmani and Belkheiri (11):

$$y_{nn_i} = \sum_{j=1}^{N_2}\left[w_{ij}\varphi_j\left(\sum_{k=1}^{N_1} v_{jk}x_k + \vartheta_{vj}\right) + \vartheta_{wi}\right] \quad (48)$$

$i = 1, \dots, N_3$ and $x \in \mathbb{R}^{N_1}$

The previous NN equation can be represented in compact form as follows (11):

$$y_{nn} = W^T\varphi(V^T x) \quad (49)$$

3. 5. Application The learning procedure can be accomplished through a diverse range of techniques, wherein the weights are iteratively adjusted until the generated output precisely matches the desired target output (31).

The Levenberg-Marquardt (LM) algorithm is widely recognized as one of the most prominent techniques for resolving least-squares problems (32). It serves as an approximation to the Newton technique aiming to achieve the speed of the second-order training without the necessity of calculating the Hessian matrix (31). Following a sequence of approximations and optimization steps, the weights are adapted using Equation 50 (33, 34):

$$W_{k+1} = W_k - (J_k^T + J_k + \mu I)^{-1}J_k e_k \quad (50)$$

The LM method is integrated into Matlab software as a function named "trainlm", Figure 5 shows the training process using the LM algorithm to train our system within the Matlab environment. Notably, we employ a hidden layer consisting of 10 neurons and conduct 1000 training epochs.

After completing the learning phase, we proceed with implementing two SHLNN blocks in Matlab/Simulink. These blocks are designed to estimate the adaptive terms u_{ad} and u_{aq}, which will be utilized to counteract the targeted disturbance terms Δd and Δq. The adaptive terms are calculated by the following equations:

$$u_{ad} = \widehat{W}^T\varphi(V_0^T\mu_d) \quad (51)$$

$$u_{aq} = \widehat{W}^T\varphi(V_0^T\mu_q) \quad (52)$$

$$\mu_d = [V_{ds2}\ Q_{s1}]^T \quad (53)$$

$$\mu_q = \left[V_{qs2}\ P_{s1}\right]^T \quad (54)$$

$\widehat{W}$ is updated according to the following low (35):

$$\dot{\widehat{W}} = -F_{dq}[2\varphi(V_0^T\mu_{dq})\tilde{\imath}_{dq} + k_{dq}(\widehat{W} - W_0)] \quad (55)$$

$$\tilde{\imath}_{dq} = i_{dqr} - i_{dq} \quad (56)$$

4. THE WIND POWER GENERATION SYSTEM

The wind power conversion system's operational range can be categorized into four distinct zones. The initial zone, (I), during low wind speeds the electricity generation is nearly impossible. In the second zone, (II), the system utilizes the MPPT algorithm to effectively manage its operations. This optimization process considers fluctuations in wind speed, thereby maximizing power production. Moving on to Zone (III), which occurs when wind speeds exceed their nominal values, the system adjusts the pitch angle to regulate the produced electric power, maintaining it at or near the nominal level. Finally, Zone (IV) represents a state of strong winds that pose a potential threat to the wind turbine. In such emergency situations, the wind turbine is promptly halted to prevent any damage or harm (2).

4. 1. Maximum Power Point Tracking Strategy (MPPT) The objective of MPPT algorithms is to observe and optimize the utilization of power generated by the WPCS (36). Numerous MPPT algorithms exist for in the realm of wind energy, each of these algorithms have their own merits and demerits. The optimal torque control (OTC) is very simple in usage, fast speed convergence and high effectiveness (37). This algorithm focuses on measuring the generator rotor's speed and computing the required torque or power instead of measuring the wind speed, the following control method is employed to ensure that the generator torque remains at its designated reference value (27):

$$T_{em\_ref} = K_{opt}\Omega_{mec}^2 \quad (57)$$

$$K_{opt} = \frac{1}{2}\frac{C_{p\_max}}{\lambda_{opt}^3}\rho\pi R_t^3\frac{1}{G^3} \quad (58)$$

The power coefficient C_p depending on the velocity ratio λ and the pitch angle β reaches its maximum value ($C_{p\_max} = 0.44$) when the pitch angle is zero, thus the velocity ratio becomes at its optimal value ($\lambda_{opt} = 7$).

Figure 6 depicts the various components of the wind turbine using a block diagram, with a specific highlight on the MPPT strategy:

4. 2. The WPGS Based on The CDFIG The process of using the CDFIG as a wind turbine generator involves several types of connections, one of them is by linking

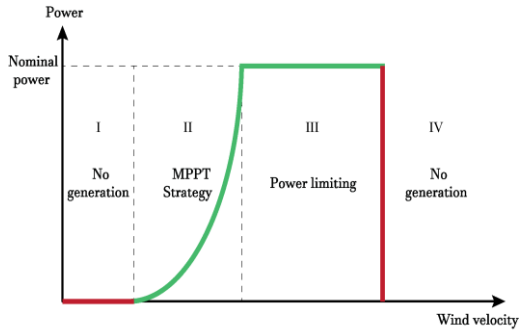

Figure 5. The operational range of the WPCS

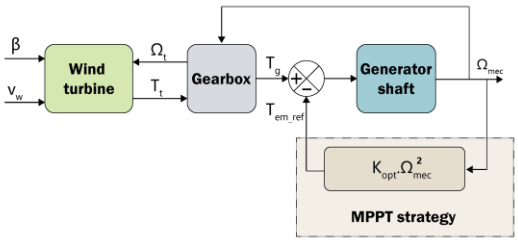

Figure 6. MPPT strategy usage in the wind turbine

the initial stator directly to the grid, while the second stator is linked to the grid via an intermediate AC/AC converter which allows the energy to be controlled and transferred in both directions (6).

The WPCS based on the CDFIG is illustrated in Figure 7.

5. RESULTS AND DISCUSSION

The parameters of the generators and the wind turbine used for the simulation have been selected from literature (25).

The simulation was done using MATLAB/Simulink environment. In the first case, the PI controller implemented alone to control the active power and reactive power. In the second case, the neural network will be added alongside to the PI controller. The results show the difference between both cases. Figure 8 shows the wind velocity profile. Rotor speed in RPM is illustrated in Figure 9.

The wind speed varies between approximately 6 m/s and 13 m/s. The pattern of changes in wind speed is irregular, with several peaks and dips, indicating variability in wind conditions.

The active power of the first generator; first case and second case controlled by the PI controller are shown in

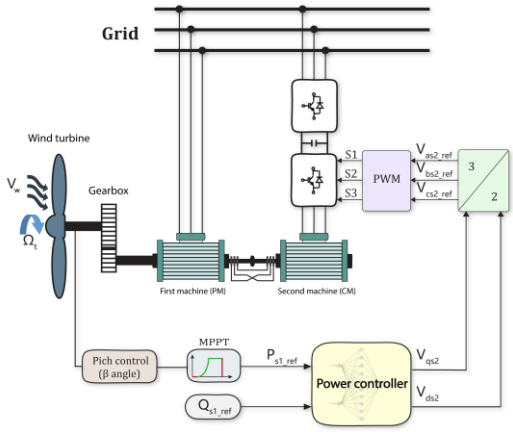

Figure 7. The WPCS based on the CDFIG

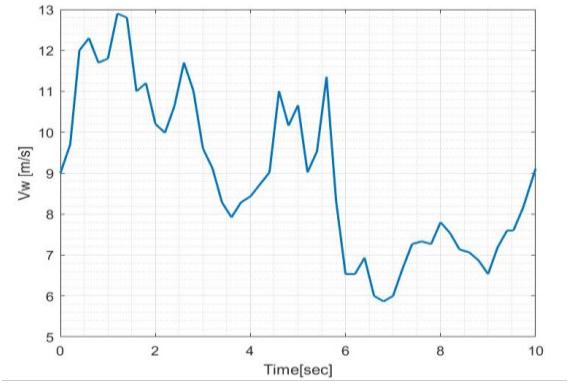

Figure 8. Wind velocity profile

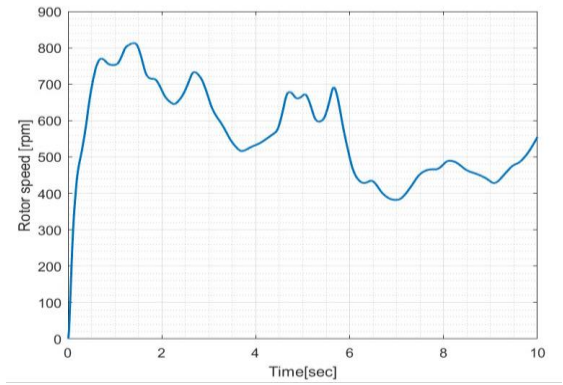

Figure 9. Rotor speed

Figures 10 and 11, respectively. The reactive power of the first generator; first case and second case are shown in Figures 12 and 13, respectively. It is evident that the active and reactive power cannot closely track their reference values during periods of rapid strong wind velocity variation as we can see in Figure 10 the power error amount to 100 kW. However, when neural network is introduced in conjunction with the PI controller, a significant enhancement in results becomes apparent. In Figure 11, the active power plot demonstrates a near-elimination of errors. This improvement is further highlighted by examining the transient response, which is markedly better in the second case. The transient response, a critical aspect of wind generation systems, demonstrates an enhanced ability to quickly and efficiently adjust to changes in wind speed and load demands. This rapid adjustment capability is vital for maintaining system stability and ensuring consistent power output. In Figure 13, the reactive power plot shows a remarkable reduction in errors by 60 KVA.

These results provide compelling justification for the accurate identification of inversion errors (Δ_q) and (Δ_d) by the adaptive terms (u_{aq}) and (u_{ad}), respectively, as depicted in Figures 14 and 15.

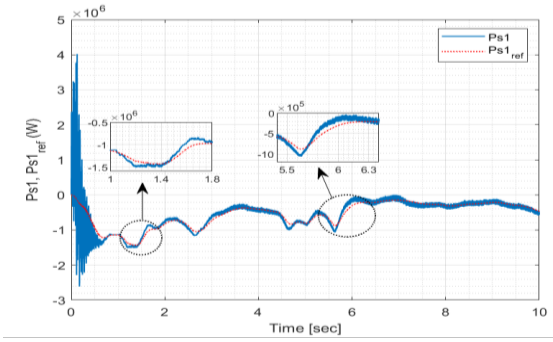

Figure 10. The active power of the first generator; first case

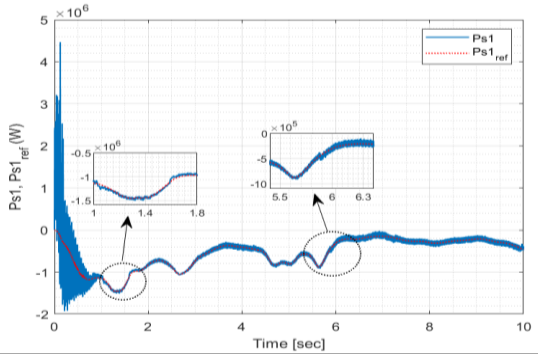

Figure 1. The active power of the first generator; second case

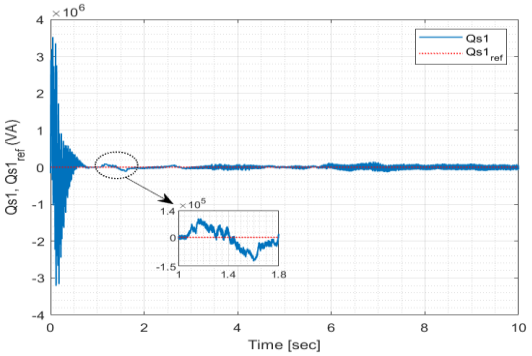

Figure 2. The reactive power of the first generator; first case

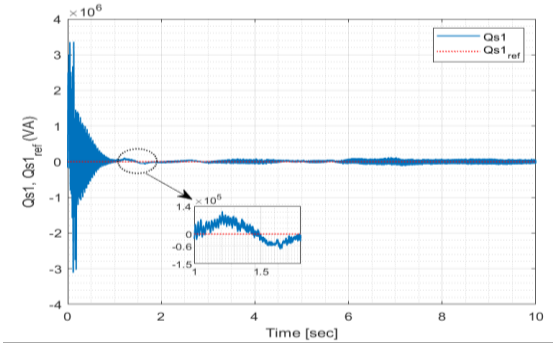

Figure 3. The reactive power of the first generator; second case

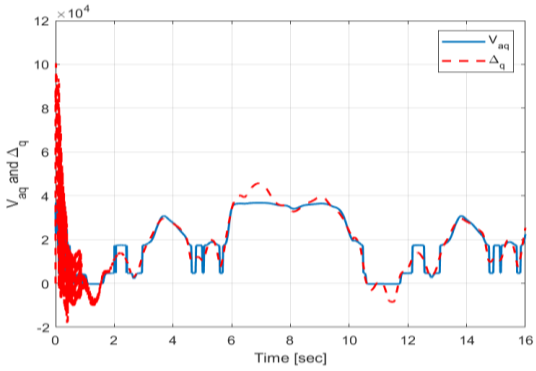

Figure 4. Identification of Δ_q by NN

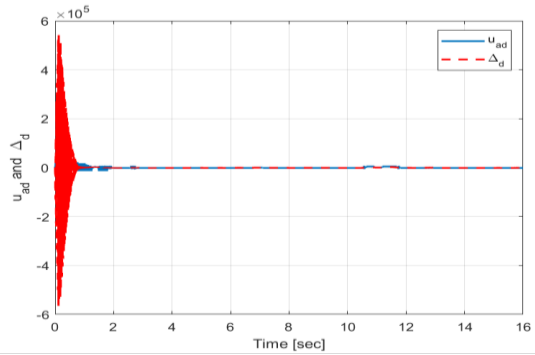

Figure 5. Identification of Δ_d by NN

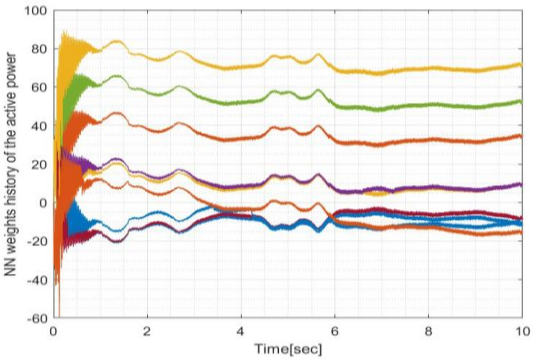

Figure 6. History of NN weights of the active power

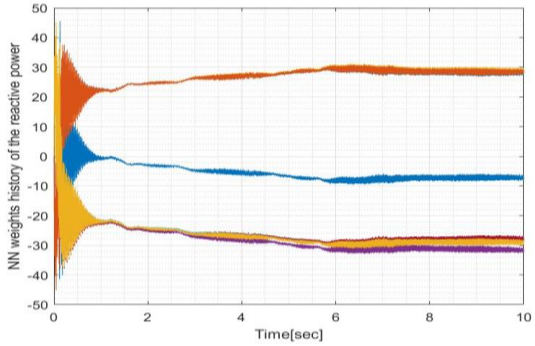

Figure 7. History of NN weights of the reactive power

The neural network weights history of the active power and the reactive power are shown in Figures 16 and 17, respectively. As observed the weights are chosen carefully and accurately to adapt with the system and to provide a better control command the values of this last are in between -40 to 40 for the NN of the reactive power and -40 to 90 and for the NN of the active power the initial weights were selected using the developer expertise and are optimized during the training session for best outcomes.

This improved performance can be attributed to the neural network's ability to predict and compensate for the system's behavior more effectively than the conventional PI controller, which is based on fixed gains and does not adapt to changing conditions dynamically.

6. CONCLUSION

The integration of neural network with a PI controller in wind generator control systems has proven to be a highly effective approach for enhancing performance, particularly in the presence of rapidly changing wind conditions. The results clearly demonstrate a remarkable reduction in errors and a significant improvement in the accuracy of power control.

This study serves as a strong foundation for the application of neural networks in renewable energy systems, offering the potential for improved efficiency and grid stability. The carefully chosen and optimized neural network weights play a critical role in adapting to system dynamics, ensuring a robust control strategy.

As the renewable energy industry continues to grow, innovative solutions like the one explored in this study will become increasingly important in harnessing the full potential of wind energy and addressing the challenges posed by variable wind conditions. It is clear that neural networks hold great promise for the future of the wind energy generation, offering a path toward more reliable and efficient power production.

7. REFERENCES

1. Strielkowski W, Civín L, Tarkhanova E, Tvaronavičienė M, Petrenko Y. Renewable Energy in the Sustainable Development of Electrical Power Sector: A Review. Energies. 2021;14(24). 10.3390/en14248240
2. Chojaa H, Derouich A, Chehaidia SE, Zamzoum O, Taoussi M, Elouatouat H. Integral sliding mode control for DFIG based WECS with MPPT based on artificial neural network under a real wind profile. Energy Reports. 2021;7:4809-24. 10.1016/j.egyr.2021.07.066
3. El Achkar M, Mbayed R, Salloum G, Monmasson E. New voltage compensation of a standalone CDFIG supplying unbalanced loads. International Journal of Electrical Power & Energy Systems. 2021;124. 10.1016/j.ijepes.2020.106396
4. Olubamiwa OI, Gule N. A Review of the Advancements in the Design of Brushless Doubly Fed Machines. Energies. 2022;15(3). 10.3390/en15030725
5. Achkar ME, Mbayed R, Salloum G, Patin N, Monmasson E. Voltage Control of a Stand-Alone Cascaded Doubly Fed Induction Generator. IEEE Transactions on Industrial Electronics. 2019;66(1):762-71. 10.1109/tie.2018.2856186
6. Nguyen D-D, Than N-H, Hoang D-T. The cascade methods of doubly-fed induction machine for generator system. International Journal of Power Electronics and Drive Systems (IJPEDS). 2021;12(1). 10.11591/ijpeds.v12.i1.pp112-120
7. Maafa A, Mellah H, Ghedamsi K, Aouzellag D. Improvement of Sliding Mode Control Strategy Founded on Cascaded Doubly Fed Induction Generator Powered by a Matrix Converter. arXiv preprint arXiv:220811140. 2022.
8. Taghinezhad J, Sheidaei S. Prediction of operating parameters and output power of ducted wind turbine using artificial neural networks. Energy Reports. 2022;8:3085-95. 10.1016/j.egyr.2022.02.065
9. Narimene K, Kheira M, Mohamed F. Robust Neural Control of Wind Turbine Based Doubly Fed Induction Generator and NPC Three Level Inverter. Periodica Polytechnica Electrical Engineering and Computer Science. 2022;66(2):191-204. 10.3311/PPee.19921
10. Vajdian M, Zahrai S, Mirhosseini S, Zeighami E. Predicting Shear Capacity of Panel Zone Using Neural Network and Genetic Algorithm. International Journal of Engineering. 2020;33(8):1512-21.
11. Rahmani B, Belkheiri M. Adaptive neural network output feedback control for flexible multi-link robotic manipulators. International Journal of Control. 2018;92(10):2324-38. 10.1080/00207179.2018.1436774
12. Kashkooli MA, Madani S, Kiyoumarsi A. Soft Grid Connection of Cascaded Doubly Fed Induction Generator Using Direct Torque & Flux Control for Wind Turbine Application. Majlesi Journal of Energy Management. 2016;5.
13. Zahedi H, Arab Markadeh G, Taghipour S. Real-time implementation of sliding mode control for cascaded doubly fed induction generator in both islanded and grid connected modes. Journal of Electrical and Computer Engineering Innovations (JECEI). 2020;8(2):285-96.
14. Svečko R, Gleich D, Sarjaš A. The Effective Chattering Suppression Technique with Adaptive Super-Twisted Sliding Mode Controller Based on the Quasi-Barrier Function; An Experimentation Setup. Applied Sciences. 2020;10(2). 10.3390/app10020595
15. Abdolhadi HZ, Markadeh GA, Boroujeni ST. Sliding mode and terminal sliding mode control of cascaded doubly fed induction generator. Iranian Journal of Electrical and Electronic Engineering. 2021;17(3):1955-.
16. Yan X, Cheng M. A Robustness-Improved Control Method Based on ST-SMC for Cascaded Brushless Doubly Fed Induction Generator. IEEE Transactions on Industrial Electronics. 2021;68(8):7061-71. 10.1109/tie.2020.3007087
17. Yu X, Feng Y, Man Z. Terminal Sliding Mode Control – An Overview. IEEE Open Journal of the Industrial Electronics Society. 2021;2:36-52. 10.1109/ojies.2020.3040412
18. Bayhan S, Kakosimos P, Rivera M, editors. Predictive torque control of brushless doubly fed induction generator fed by a matrix converter. 2018 IEEE 12th International Conference on Compatibility, Power Electronics and Power Engineering (CPE-POWERENG 2018); 2018: IEEE.
19. Abdolrahimi H, Arab Khaburi D. A novel model predictive voltage control of brushless cascade doubly-fed induction

generator in stand-alone power generation system. International Journal of Engineering. 2021;34(5):1239-49.

20. Dauksha G, Iwanski G. Indirect Torque Control of a Cascaded Brushless Doubly-Fed Induction Generator Operating With Unbalanced Power Grid. IEEE Transactions on Energy Conversion. 2020;35(2):1065-77. 10.1109/tec.2020.2972500
21. Morales LA, Fabara P, Pozo DF. An Intelligent Controller Based on LAMDA for Speed Control of a Three-Phase Inductor Motor. Emerging Science Journal. 2023;7(3):676-90. 10.28991/esj-2023-07-03-01
22. Ismaiel A. Wind Turbine Blade Dynamics Simulation under the Effect of Atmospheric Turbulence. Emerging Science Journal. 2022;7(1):162-76. 10.28991/esj-2023-07-01-012
23. Mahmoudabadi A, Kanaani M, Pourhossein Ghazimahalleh F. Modifying Hidden Layer in Neural Network Models to Improve Prediction Accuracy: A Combined Model for Estimating Stock Price. HighTech and Innovation Journal. 2022;3(1):45-55. 10.28991/hij-2022-03-01-05
24. Thaghipour Boroujeni S. Complex vector modeling of a doubly fed cascaded cage rotor induction machine. Electrical Engineering. 2020;102(3):1831-42. 10.1007/s00202-020-00996-7
25. Maafa A, Aouzellag D, Ghedamsi K, Abdessemed R. Cascaded doubly fed induction generator with variable pitch control system. Rev Roum Sci Techn–Électrotechn et Énerg. 2016;61(4):361-6.
26. Yan X, Cheng M, editors. A robust grid synchronization method for cascaded brushless doubly fed induction generator. 2019 22nd International Conference on Electrical Machines and Systems (ICEMS); 2019: IEEE.
27. Dahbi A, Reama A, Hamouda M, Nait-Said N, Nait-Said M-S. Control and study of a real wind turbine. Computers & Electrical Engineering. 2019;80. 10.1016/j.compeleceng.2019.106492
28. Kelkoul B, Boumediene A. Stability analysis and study between classical sliding mode control (SMC) and super twisting algorithm (STA) for doubly fed induction generator (DFIG) under wind turbine. Energy. 2021;214. 10.1016/j.energy.2020.118871
29. Boubzizi S, Abid H, El Hajjaji A, Chaabane M. Comparative study of three types of controllers for DFIG in wind energy conversion system. Protection and Control of Modern Power Systems. 2018;3:1-12.
30. El Hamidi K, Mjahed M, El Kari A, Ayad H. Adaptive Control Using Neural Networks and Approximate Models for Nonlinear Dynamic Systems. Modelling and Simulation in Engineering. 2020;2020:1-13. 10.1155/2020/8642915
31. Nazaré G, Castro R, Gabriel Filho LRA. Wind power forecast using neural networks: Tuning with optimization techniques and error analysis. Wind Energy. 2019;23(3):810-24. 10.1002/we.2460
32. Wang M, Xu X, Yan Z, Wang H. An online optimization method for extracting parameters of multi-parameter PV module model based on adaptive Levenberg-Marquardt algorithm. Energy Conversion and Management. 2021;245. 10.1016/j.enconman.2021.114611
33. Ye Z, Kim MK. Predicting electricity consumption in a building using an optimized back-propagation and Levenberg–Marquardt back-propagation neural network: Case study of a shopping mall in China. Sustainable Cities and Society. 2018;42:176-83. 10.1016/j.scs.2018.05.050
34. Peiris AT, Jayasinghe J, Rathnayake U, Vallée F. Forecasting Wind Power Generation Using Artificial Neural Network: "Pawan Danawi"—A Case Study from Sri Lanka. Journal of Electrical and Computer Engineering. 2021;2021:1-10. 10.1155/2021/5577547
35. Abbas HA, Belkheiri M, Zegnini B. Feedback linearisation control of an induction machine augmented by single-hidden layer neural networks. International Journal of Control. 2016;89(1):140-55.
36. Le XC, Duong MQ, Le KH. Review of the Modern Maximum Power Tracking Algorithms for Permanent Magnet Synchronous Generator of Wind Power Conversion Systems. Energies. 2022;16(1). 10.3390/en16010402
37. Apata O, Oyedokun DTO. An overview of control techniques for wind turbine systems. Scientific African. 2020;10. 10.1016/j.sciaf.2020.e00566

Persian Abstract

چکیده

این مشارکت با هدف بهبود محدودیت‌های یک کنترل‌کننده متعارف تناسبی-انتگرالی-مشتقی (PID) با یکپارچه سازی یک شبکه عصبی تک لایه پنهان (SHLNN) در سیستم کنترل انجام شده است. به‌ویژه، در سیستم تبدیل انرژی بادی (WPGS) بر اساس مولد القایی دوبل تغذیه شده با کاسکاد .(CDFIG) هدف از این یکپارچه‌سازی کاهش ضررهای انرژی ناشی از ناپایداری و نادقیقی‌های سیستم‌های سنتی است که به واسطه محدودیت‌های باد ایجاد می‌شوند. علاوه بر این، این روش در جستجوی بهره‌برداری از مزایای مولد القایی دوبل تغذیه شده با کاسکاد (CDFIG) و شبکه عصبی مصنوعی در کنترل WPCS است. در حالی که کنترل‌کننده PI همچنان مکانیزم کنترل اصلی است، محدودیت‌های آن به دلیل غیرخطی بودن و عدم قطعیت‌های WPCS توسط قابلیت‌های تطبیق‌پذیر و پیچیدگی محاسباتی پایین SHLNN مورد توجه قرار گرفته است. این رویکرد از توانایی یادگیری رابطه‌های غیرخطی شبکه‌های عصبی استفاده می‌کند، که با استفاده از داده‌های تاریخی سرعت باد و تولید انرژی آموزش داده شده‌اند، تا به طور مؤثر با تغییرات ذاتی الگوهای باد روبرو شوند. شبیه‌سازی‌ها با استفاده از Matlab/Simulink انجام می‌شوند تا عملکرد کنترل‌کننده PI با یک پیاده‌سازی شبکه عصبی تکی مقایسه شود. در نهایت، نتایج شبیه‌سازی ارائه و به طور کامل تحلیل می‌شوند و بینش‌هایی در مورد اثربخشی رویکرد پیشنهادی ارائه می‌دهند.